# Direct observation of spin polarization in epitaxial $Fe_3O_4$(001)/MgO thin films grown by magnetron sputtering

Zhe Zhang,[1, #] Xianyang Lu, [1, 2, #, a)] Yu Yan,[1, 2] Jiahua Lu,[1] Zhuoyi Li,[1] Qi Liu,[1] Fangyuan Zhu,[3] Jiefeng Cao,[3] Yong Wang,[3] Zhaocong Huang,[4] Ya Zhai,[4] Yao Li,[1] Xuezhong Ruan,[1] Liang He,[1] Jing Wu[2], Jun Du,[5] Rong Zhang[1], Yongbing Xu[1, 2, a)]

[1]*Jiangsu Provincial Key Laboratory of Advanced Photonic and Electronic Materials, School of Electronic Science and Engineering, Nanjing University, Nanjing 210093, China*

[2]*York-Nanjing International Joint Center in Spintronics, Department of Electronics and Physics, University of York, York YO10 5DD,* of *UK*

[3]*Shanghai Synchrotron Radiation Facility, Shanghai Advanced Research Institute, Chinese Academy of Sciences, Shanghai 201204, China*

[4]*Department of Physics, Southeast University, Nanjing 211189, China*

[5]*Department of Physics, Nanjing University, Nanjing 210093, China*

**We obtained epitaxial single-crystal $Fe_3O_4$(001)/MgO(001) thin films by magnetron sputtering. The high quality of the grown $Fe_3O_4$ films was confirmed by reflection high-energy electron diffraction (RHEED) and X-ray photoelectron spectroscopy (XPS). The atomic magnetic properties of $Fe_3O_4$(001)/MgO(001) were investigated using vibrating sample magnetometry (VSM) and X-ray magnetic circular dichroism (XMCD). The values of saturation magnetization and magnetic moment are 407±5 emu/cm$^3$ (3.26±0.04 $\mu_B/(f.u.)$) and 3.31±0.15 $\mu_B/(f.u.)$ in the $Fe_3O_4$ film as thin as 5 nm, which are close to the bulk values. The spin polarization was directly measured using spin-resolved photoemission spectroscopy (SRPES). The measured spin polarization has a maximum value of -42±3%, which is comparable to the theoretical value for the (√2×√2)R45° reconstructed $Fe_3O_4$(001) surface. Furthermore, the film thickness-dependent measurements indicate that the anti-phase boundaries (APBs) significantly decrease the spin polarization rather than the lattice mismatch. Our results demonstrate that the epitaxial $Fe_3O_4$(001)/MgO thin films grown by magnetron sputtering have desired magnetic properties, facilitating the potential application of $Fe_3O_4$-based spintronic devices.**

[a)]Authors to whom correspondence should be addressed: xylu@nju.edu.cn and ybxu@nju.edu.cn

[#]Z. Zhang and X. Lu contributed equally to this work

In the past few decades, great progress has been made in the research field of spintronic devices. In these devices, effective injection and detection of spin-polarized currents via ferromagnetic (FM) materials are the key. Half-metallic ferromagnets (HMFs), owing to their predicted 100% spin polarization at the Fermi level, have attracted great attention since it was first proposed in the early 1980s[1]. Among HMF materials, magnetite ($Fe_3O_4$) has attracted more attention due to its stability at high temperatures. Moreover, $Fe_3O_4$ exhibits robust ferrimagnetism with a Curie temperature $T_C$=851 K. A 100% spin polarization near the Fermi level ($E_F$) is theoretically predicted in $Fe_3O_4$ with a conductive minority spin channel and a semiconducting majority spin channel[2,3]. This makes $Fe_3O_4$ attract more interest as a potential material for next-generation spintronic devices[4-6].

$Fe_3O_4$ films can be prepared by three methods: pulsed laser deposition (PLD)[7], molecular beam epitaxy (MBE)[8], and magnetron sputtering. Compared with the other two methods, the magnetron sputtering method is easy to implement, simple and efficient. The films grown by magnetron sputtering are generally more compact and uniform. Therefore, it is more convenient to use in device fabrication and industrial production. Yanagihara *et al*. grew spinel-type epitaxial $Fe_3O_4$(001) films using reactive sputtering by introducing $O_2$ gas into an Ar base gas during film growth in a radio frequency (RF) planar magnetron sputtering apparatus[9]. However, studies on spin polarization and atomic magnetization in $Fe_3O_4$ films prepared by magnetron sputtering are limited.

In this work, high-quality epitaxial $Fe_3O_4$(001) thin films grown on MgO(001) substrates using RF magnetron sputtering were confirmed by a series of characterization experiments. The values of the magnetization and the atomic moment are found to be close to the bulk values when the film thickness is larger than 5 nm. A maximum value of spin polarization of -42±3% is observed for 40 nm $Fe_3O_4$(001) films, which is close to the theoretically predicted value. Importantly, the thickness-dependent measurements demonstrate that the spin polarization of the nanoscale $Fe_3O_4$(001)/MgO films is significantly affected by the anti-phase boundary defects rather than the lattice mismatch.

High-quality $Fe_3O_4$ (001) films were grown on single-crystal MgO(001) substrates by introducing $O_2$ gas into an Ar base gas during film growth in our magnetron sputtering system with a base pressure of $1 \times 10^{-8}$ Torr. The MgO(001) substrates were annealed at 500 °C for 60 min until a smooth surface could be identified via the sharp reflection high-energy electron diffraction (RHEED) patterns, as shown in Fig. 1(a). During the film growth process, a 50 sccm Ar (99.999%) gas flow was introduced, while the flow rate of $O_2$ (99.999%) was controlled from 0.0 to 2.0 sccm. The total gas pressure was maintained at about $4 \times 10^{-3}$ Torr. A pure iron target (99.95%) was used, and the RF power was set as 50 W. The substrate temperature was fixed at 300 °C during the deposition process. After deposition, RHEED measurements were *in-situ* performed. By measuring the spacing of the streaks in RHEED images using KSA 400 software, we can determine the lattice constant of films with different lattice structures. The structural and elemental analysis of the grown films were *ex-situ* carried out by X-ray

diffraction (XRD), X-ray photoelectron spectroscopy (XPS) and Raman spectroscopy.

The grown films were immediately transferred from the growth chamber to the spin-resolved photoemission spectroscopy (SRPES) chamber via a UHV ($5 \times 10^{-10}$ Torr) interconnected tube. Thus, the SRPES measurements can be *in-situ* performed on a high-quality sample surface. The base pressure of the analyzer chamber is under $2 \times 10^{-10}$ mbar, and the energy resolution is 35 meV at room temperature. A helium lamp is applied to generate ultraviolet light with a photon energy of 21.218 eV (He-I). All SRPES measurements were performed at room temperature.

The static magnetic hysteresis loops along the MgO[0-11] direction are measured by a vibrating sample magnetometer (VSM) at room temperature. X-ray magnetic circularly dichroism (XMCD) measurements at the Fe $L_{2,3}$ absorption edges were performed at beamline BL07U of the Shanghai Synchrotron Radiation Facility. The X-ray absorption (XAS) was measured at room temperature under an applied magnetic field of 3 T along the out-of-plane direction by total electron yield (TEY) detection. The 100% circularly polarized X-rays were used in normal incidence with respect to the sample plane and in parallel with the applied magnetic field. By flipping the X-ray helicity at a fixed magnetic field, we can obtain the XMCD of our samples.

It is well known that both the rock salt structure of MgO and the inverse spinel structure of $Fe_3O_4$ are based on a fcc oxygen anion lattice. This allows a continuous oxygen sublattice over the MgO/$Fe_3O_4$ interface[10]. The lattice constant of $Fe_3O_4$ 8.396 Å is approximately twice that of MgO 4.216 Å, resulting in a very small lattice mismatch. As shown in Fig. 1(b), a clear and sharp RHEED pattern indicates that the

Fe film deposited with a 0 sccm $O_2$ flow rate has a bcc structure with an epitaxial relationship of Fe(001)[0-11]//MgO(001)[001]. Fig. 1(c) shows the RHEED pattern of the 20 nm $Fe_3O_4$ film grown on a MgO(001) substrate at an $O_2$ flow rate of 1.5 sccm with an epitaxial relationship of $Fe_3O_4$(001)[001]//MgO(001)[001]. The image confirms a specific $(\sqrt{2}\times\sqrt{2})$R45° reconstruction of the $Fe_3O_4$(001) surface[11]. Clear and sharp lines with a Laue ring also confirm that our grown film exhibits good crystallinity with a flat well-ordered surface. When the $O_2$ flow rate increased to 2 sccm, we obtained a γ-$Fe_2O_3$ film, as shown in Fig. 1(d). It is worth mentioning that the ε-$Fe_2O_3$ phase will not occur unless the growth temperature increases to 800 ℃[12].

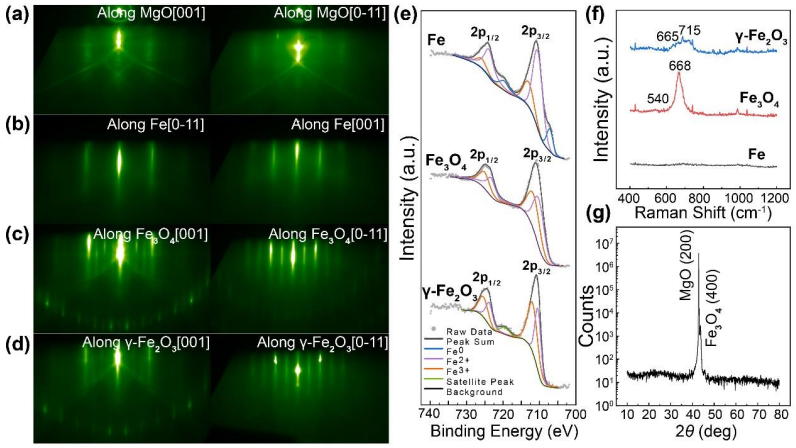


FIG 1. RHEED patterns of the (a) MgO(001) substrate. (b) 20 nm Fe film grown at 0 sccm flow rate of $O_2$. (c) 20 nm $Fe_3O_4$ film grown at 1.5 sccm flow rate of $O_2$. (d) 20 nm γ-$Fe_2O_3$ film grown at a 2 sccm flow rate of $O_2$. (e) Fe 2p XPS spectra of 20 nm Fe, $Fe_3O_4$, and γ-$Fe_2O_3$ films. (f) Raman spectra of 20 nm Fe, $Fe_3O_4$, and γ-$Fe_2O_3$ films. (g) XRD spectrum of 50 nm $Fe_3O_4$ film.

The Fe 2p core-level XPS spectra of the films deposited at different $O_2$ flow rates

are presented in Fig. 1(e). The XPS spectra were fitted by using XPS peak 4.1 software. As shown in the middle row, the spectrum of a 20 nm $Fe_3O_4$ film deposited at 1.5 sccm of $O_2$ shows two $Fe_3O_4$ characteristic peaks at 711 and 724 eV, corresponding to the binding energies of $Fe^{2+}$ $2p_{3/2}$ and $Fe^{2+}$ $2p_{1/2}$[13,14]. The films were also analyzed by Raman spectroscopy, as shown in Fig. 2(f). We can observe one major component situated at 668 $cm^{-1}$ and a minor component at approximately 540 $cm^{-1}$ for $Fe_3O_4$. The major Raman peaks for γ-$Fe_2O_3$ appear at 665 $cm^{-1}$ and 715 $cm^{-1}$, which are in good agreement with the results obtained in other studies[15,16]. We also carried out XRD measurements of a 50 nm $Fe_3O_4$ film. As shown in Fig. 1(g), the observation of clear and sharp MgO (200) and $Fe_3O_4$ (400) peaks confirms that our $Fe_3O_4$ films have a good (001) orientation. Through the above analysis, we can observe a clear oxidation process, and the best flow rate of $O_2$ for $Fe_3O_4$ growth is 1.5 sccm.

The magnetic hysteresis loops as a function of the $Fe_3O_4$ film thickness with an applied magnetic field along the MgO[0-11] direction are shown in Fig. 2(b). The $M_S$ increases with the thickness and reaches a maximum of 407±5 emu/$cm^3$ (3.26±0.04 $\mu_B/(f.u.)$) at 5 nm, which is lower than the value of 480 emu/$cm^3$ for bulk magnetite. The Fe $L_{2,3}$-edge XAS and XMCD spectra of films deposited at 0, 1.5, and 2 sccm $O_2$ are shown in Fig. 2(a). For $Fe_3O_4$, due to the antiparallel spin orientations of the A and B sites, the characteristic contributions from different sites of $Fe_{td}^{3+}$, $Fe_{oh}^{2+}$, and $Fe_{oh}^{3+}$ in $Fe_3O_4$ can be identified. For γ-$Fe_2O_3$, the XMCD signal was derived from the superposition of the contributions of $Fe^{3+}$ ions at both the A and B sites[17]. All of the measured XMCD spectra are in agreement with reported studies[17-19]. The values of spin

moment $m_s$ and orbital moment $m_l$ were calculated by applying sum rules on the integrated XMCD and total XAS spectra of Fe $L_{2,3}$ edges based on Eq. (1),

$$m_l = -\frac{4}{3} n_h \frac{\int_{L_{2,3}} (\sigma^+ - \sigma^-) dE}{\int_{L_{2,3}} (\sigma^+ + \sigma^-)\, dE}$$

$$m_s + \langle T_z \rangle = -n_h \frac{6\int_{L_3} (\sigma^+ - \sigma^-) dE - 4\int_{L_{2,3}} (\sigma^+ - \sigma^-)\, dE}{\int_{L_{2,3}} (\sigma^+ + \sigma^-)\, dE}, \quad (1)$$

where $n_h = 6.61$ is the effective number of 3d-band holes[19]. The magnetic dipole term $\langle T_Z \rangle$ is negligible because of the predominantly cubic symmetry of magnetite. The background of each XAS spectrum was fitted by an arctangent-based step function[20], as shown in Fig. 2(a). From the 5 nm $Fe_3O_4$ film deposited at an $O_2$ flow rate of 1.5 sccm, we obtained the values of $m_s = 2.64 \pm 0.1\ \mu_B/\text{f.u.}$ and $m_l = 0.67 \pm 0.05\ \mu_B/\text{f.u.}$, while the total moment $m_{l+s} = 3.31 \pm 0.15\ \mu_B/\text{f.u.}$ and the orbital to spin moment ratio $m_l/m_s = 0.25$. The epitaxial $Fe_3O_4$/MgO(001) thin film exhibits a considerably large $m_l$, but its $m_{l+s}$ is less than the bulk value ($4.0\ \mu_B/(f.u.)$). Table SI gives an overview of the spin and orbital moment of the magnetite. Among these results, Babu et al. observed a sizeable $m_l = 0.44 \pm 0.05\ \mu_B/\text{f.u.}$ in $Fe_3O_4/BaTiO_3$[21], while an unquenched $m_l$ of $0.47 \pm 0.05\ \mu_B/\text{f.u.}$ was also observed by Liu et al. in $Fe_3O_4$/MgO/GaAs[18]. Our results are in good agreement with these works, and the observation of a large $m_l$ is of significance for spintronics applications as high <LS> coupling is essential for the ultrafast switching of spin polarization by electric field and circularly polarized light[22-25].

Fig. 2(c) shows the saturation magnetization ($M_S$) and atomic magnetic moment of $Fe_3O_4$ films deposited at 1.5 sccm with different film thicknesses. The $M_S$ and

magnetic moment increase as a function of film thickness and reach maximum values at a thickness of 5 nm. This observation is consistent with the lattice constant data shown in Fig. 4. It is indicated that when the thickness is less than 5 nm, the lattice mismatch between the grown layer and the substrate is larger, resulting in a corresponding decrease in the $M_S$ and magnetic moment. Another reason for the low $M_S$ and magnetic moment in thin films may be the interdiffusion between $Mg^{2+}$ and Fe ions at the interface[26]. Our films are grown at 300°C, so this diffusion is to be expected. The maximum values of $M_S$ and the magnetic moment we observed are reduced compared with the bulk values, which may be due to the formation of antiphase boundaries (APBs) in $Fe_3O_4$. Such antiferromagnetic exchange interactions between the boundaries usually lead to a saturation field as large as 7 T[18,27,28]. Our applied magnetic field of 3 T is not large enough to rule out the effects of APBs during our measurements. The values of $M_S$ are in line with the value of the magnetic moment after converting emu/cm$^3$ to $\mu_B$/f. u. when the thickness reaches 5 nm. However, the minimum value of the magnetic moment at 1 nm ($1.80 \pm 0.05$ $\mu_B$/f. u.) is smaller than the value of $M_S$ ($2.82 \pm 0.04$ $\mu_B$/f. u.). This provides further evidence that APBs play a significant role in the measurements of XMCD when the $Fe_3O_4$ thickness is relatively small. Nevertheless, it is clearly shown that the values of magnetization and the atomic moment change obviously with film thickness. When the thickness of our grown $Fe_3O_4$ reaches 5 nm, the values of $M_s$ and the total magnetic moment are close to the bulk value.

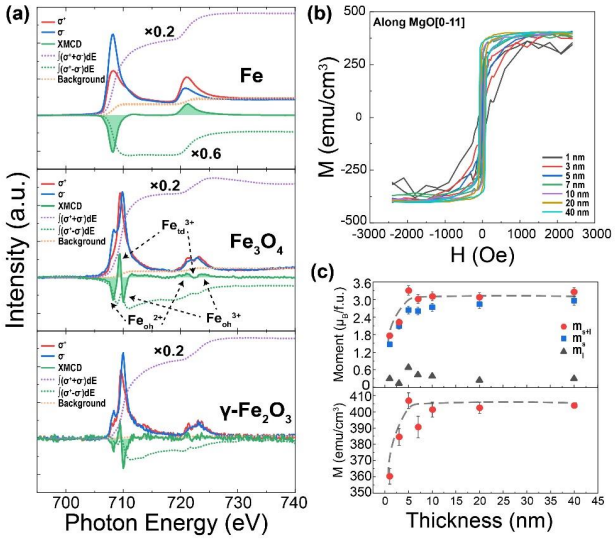


FIG 2. (a) Fe $L_{2,3}$-edge XAS and XMCD spectra of 20 nm Fe (0 sccm $O_2$), 5 nm $Fe_3O_4$ (1.5 sccm $O_2$) and 20 nm γ-$Fe_2O_3$ (2 sccm $O_2$). (b) VSM magnetization curves of $Fe_3O_4$ films with different thicknesses. (c) $M_S$ and moment of $Fe_3O_4$ films with different thicknesses. The dashed lines are guidelines for the eye.

SRPES measurements were *in-situ* performed, and the spin polarization P is defined as $P = \frac{1}{S_{eff}} \frac{I_+ - I_-}{I_+ + I_-}$, where the effective Sherman function $S_{eff}$ = 0.16±0.01 is used and $I_+$ and $I_-$ are the spectra acquired by the two channeltrons in opposite spin directions. The SRPES spectra and the corresponding spin polarization of $Fe_3O_4$ films with different thicknesses are shown in Fig. 3. The spin polarization changed dramatically with the $Fe_3O_4$ thickness. When the thickness increased to 5 nm, we can observe a typical spin polarization curve of $Fe_3O_4$. The 40 nm $Fe_3O_4$ film deposited at 1.5 sccm has a spin polarization value up to -42±3% near the Fermi level. The absolute value of the spin polarization decreases and switches sign at 1.0 eV. It exhibits a maximum value with further increasing binding energies and becomes negative again

at 1.8 eV. Our results are in good agreement with the theoretically predicted values of spin polarization at the Fermi level, considering surface reconstruction and stabilization[29]. The surfaces of magnetite tend to reconstruct due to their polar nature, and thus their magnetic and electronic properties may strongly deviate from each other and from the bulk. The intrinsic instability of the magnetite (100) and (111) surfaces is known to result in a variety of possible metastable reconstructions[30]. For $Fe_3O_4$ (001), a larger $(\sqrt{2} \times \sqrt{2})R45°$ reconstruction was observed experimentally[11,31] instead of the $(1 \times 1)$ bulk-like termination. The atomic structure of this reconstruction surface is terminated by octahedrally coordinated iron atoms arranged in rows, referred to as a *modified B layer*[29,32]. From the RHEED patterns shown in Fig. 1(c), we observed a specific $(\sqrt{2} \times \sqrt{2})$R45° reconstruction of the $Fe_3O_4$(001) surface, similar to other reports[11]. The reconstruction and stabilization of the (001) surface lead to lattice distortions and consequently change the electronic properties. The DFT results reported by M. Foini et al. on the $Fe_3O_4$(001) surface show a smaller value of -40% of the spin polarization at the Fermi level ($E_F$) compared to the bulk density of state[29], which agrees very well with our results. The spin polarization close to $E_F$ reported by W. Wang *et al*. reaches −50% and −72% for 6.20 and 4.65 eV photons, respectively[33]. The high value of spin polarization they observed can be explained by an increase of the inelastic mean-free path. When a light source with lower photon energy is used, the inelastic mean-free path of electrons will increase, which could lead to a more efficient probe of bulk properties. The effect of self-energy renormalization on the majority spin states near $E_F$, resulting in an increase in spectral functions, can also reduce the spin polarization[34].

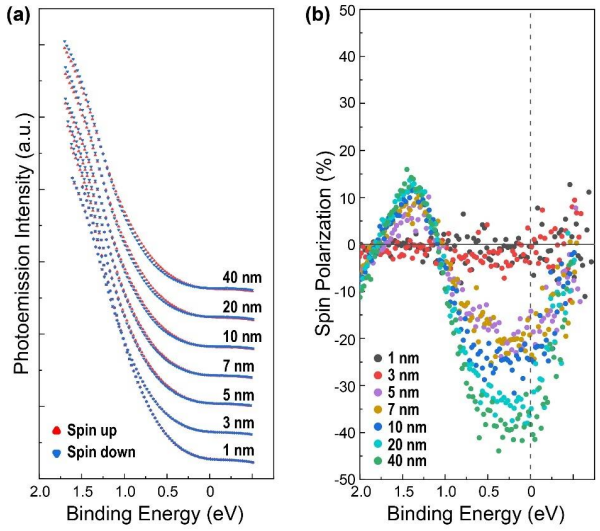


FIG 3. (a) Spin-resolved photoemission spectra of $Fe_3O_4$ (1.5 sccm $O_2$) with different thicknesses. (b) Spin polarization of $Fe_3O_4$ with different thicknesses.

The spin polarization of $Fe_3O_4$(001) films with respect to the film thickness is investigated. As shown in Fig. 4(a), the spin polarization increases with increasing thickness. Specifically, the spin polarization is almost zero at 1 nm. When the $Fe_3O_4$ thickness increases to 5 nm, the spin polarization increases significantly to -22±3%. Correspondingly, the lattice constant significantly changes at a thickness of 5 nm, as shown in the inset of Fig. 4(a), which means a decrease in lattice distortion. This result suggests a strong effect on the electronic properties caused by lattice distortions, which reduce the spin polarization in ultrathin $Fe_3O_4$ (001) films. Then, the value of spin polarization increases to -38±5% at a thickness of 20 nm and reaches -42±3% at a

thickness of 40 nm. However, when the thickness is larger than 5 nm, the lattice constant is almost unchanged and close to the bulk value of $Fe_3O_4$. This suggests that lattice distortion is not the reason for the spin polarization change when the film thickness is larger than 5 nm. As reported by Liu et al., the measured magnetoresistance decreases from −6.5% to −1.1% as the thickness of $Fe_3O_4$ decreases from 80 to 5 nm, which is explained by the enhanced spin-flip scattering at film and grain surfaces[35]. This enhanced spin-flip scattering could also account for the reduced spin polarization in thinner films. Another factor is the antiphase boundaries (APBs), which are common in magnetite films[36-38]. The SRPES measurements were performed in the remanent ($M_r$) state after being magnetized along the in-plane MgO[0-11] direction. The exchange coupling between the APBs defects is antiferromagnetic, therefore a higher $M_r$ reflects a lower density of APBs. The film thickness dependence of $M_r$, shown in Fig. 4(b), is in good agreement with the observed spin polarization. The remanence, as well as the spin polarization, reach its maximum values at about 20 nm. Therefore, the APBs play a significant role in the measurements of spin polarization, especially when the film thickness is less than a critical value of 20 nm. Nevertheless, the spin polarization of the $Fe_3O_4$ film close to the theoretical value is observed in the film as thin as 20 nm. When the film thickness is larger than the critical thickness, the magnetron sputtering grown $Fe_3O_4$ films have ideal magnetic properties close to the bulk values, including the magnetic hysteresis loops and the spin polarization near the Fermi level.

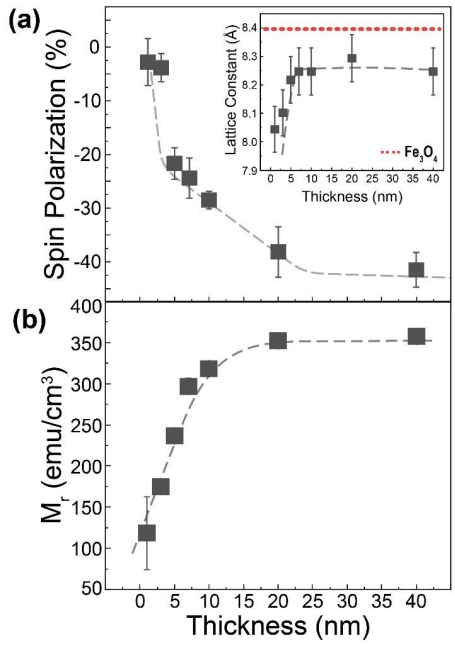


FIG 4. (a) Spin polarization near the Fermi level of $Fe_3O_4$ (1.5 sccm $O_2$) films with different thicknesses. Illustration: Lattice constant of $Fe_3O_4$ films with different thicknesses. (b) Remanence ($M_r$) of $Fe_3O_4$ films with different thicknesses. The dashed lines are guidelines for the eye.

To summarize, we have demonstrated the epitaxial growth of single-crystal $Fe_3O_4$(001) ultrathin films on MgO(001) substrates by sputtering an iron target in an Ar-$O_2$ mixed gas. The flow rate near 1.5 sccm of $O_2$ is the optimal condition for growing $Fe_3O_4$ films. The formation of high-quality ferrimagnetic $Fe_3O_4$ was confirmed by RHEED and XPS. The VSM and XMCD results show that when the thickness of the $Fe_3O_4$ film reaches 5 nm, the value of $M_s$ and the total magnetic moment are $407\pm5$ emu/cm$^3$ ($3.26\pm0.04\ \mu_B/(f.u.)$) and $3.31\pm0.15\ \mu_B/(f.u.)$, respectively, which are close to the bulk value. The spin polarization at the Fermi level is directly measured

using SRPES. The value of spin polarization changes from positive to negative to almost zero, indicating that the oxidation degree of the deposited films is gradually enhanced. A spin polarization value close to the theoretical value is observed in the $Fe_3O_4$ film as thin as 20 nm. The spin polarization has a maximum value of -42±3% for the 40 nm $Fe_3O_4$(001) film. Furthermore, the film thickness-dependent measurements indicate that the APBs significantly decrease the spin polarization rather than the lattice mismatch. Our results demonstrate the direct observation of spin polarization in epitaxial $Fe_3O_4$(001)/MgO thin films grown by magnetron sputtering, which provides some insight into the development of $Fe_3O_4$-based spintronic devices.

## SUPPLEMENTARY MATERIAL

See the supplementary material for additional information of the fitting process of XPS spectra, magnetic characterization of the samples grown at different flow fates of $O_2$, the measurements of the SRPES, and the SRPES spectra and the corresponding spin polarization of the samples grown at different flow fates of $O_2$.

## ACKNOWLEDGEMENTS

This work is supported by the National Key Research and Development Program of China (Grant Nos. 2021YFB3601600), the National Natural Science Foundation of China (Grant Nos. 12104216 and 61427812), and the Natural Science Foundation of Jiangsu Province of China (Nos. BK20200307, BK20192006, and BK20180056). The authors would like to thank the staff from BL07U beamline of the Shanghai

Synchrotron Radiation Facility (SSRF) for assistance with XMCD/XAS data collection.

## DATA AVAILABILITY

The data that support the findings of this work are available from the corresponding author upon reasonable request.

## References

[1]R. A. de Groot, F. M. Mueller, P. G. van Engen, and K. H. J. Buschow, Phys. Rev. Lett. **50**, 2024 (1983).
[2]Z. Zhang and S. Satpathy, Phys. Rev. B **44**, 13319 (1991).
[3]Yu S. Dedkov, U. Rüdiger, and G. Güntherodt, Phys. Rev. B **65** (2002).
[4]Manuel Bibes, Javier E. Villegas, and Agnès Barthélémy, Adv. Phys. **60**, 5 (2011).
[5]H. C. Wu, O. N. Mryasov, M. Abid, K. Radican, and I. V. Shvets, Sci. Rep. **3**, 1830 (2013).
[6]Shwetha G. Bhat and P. S. Anil Kumar, Mater. Res. Express **3** (2016).
[7]J. M. De Teresa, A. Fernández-Pacheco, L. Morellon, J. Orna, J. A. Pardo, D. Serrate, P. A. Algarabel, and M. R. Ibarra, Microelectron. Eng. **84**, 1660 (2007).
[8]Y. X. Lu, J. S. Claydon, Y. B. Xu, S. M. Thompson, K. Wilson, and G. van der Laan, Phys. Rev. B **70** (2004).
[9]H. Yanagihara, M. Myoka, D. Isaka, T. Niizeki, K. Mibu, and E. Kita, J. Phys. D: Appl. Phys. **46** (2013).
[10]Tatsuo Fujii, Mikio Takano, Rintaro Katano, Yasuhito Isozumi, and Yoshichika Bando, J. Magn. Magn. Mater. **130**, 267 (1994).
[11]D. J. Huang, C. F. Chang, J. Chen, L. H. Tjeng, A. D. Rata, W. P. Wu, S. C. Chung, H. J. Lin, T. Hibma, and C. T. Chen, J. Magn. Magn. Mater. **239**, 261 (2002).
[12]Victor Ukleev, Mikhail Volkov, Alexander Korovin, Thomas Saerbeck, Nikolai Sokolov, and Sergey Suturin, Phys. Rev. Mater. **3** (2019).
[13]D. Wilson and M. A. Langell, Appl. Surf. Sci. **303**, 6 (2014).
[14]Toru Yamashita and Peter Hayes, J. Electron Spectrosc. **152**, 6 (2006).
[15]C. Ruby, B. Humbert, and J. Fusy, Surf. Interface Anal. **29**, 377 (2000).
[16]D. L. A. de Faria, S. Venâncio Silva, and M. T. de Oliveira, J. Raman Spectrosc. **28**, 873 (1997).
[17]S. Brice-Profeta, M. A. Arrio, E. Tronc, N. Menguy, I. Letard, C. Cartier dit Moulin, M. Noguès, C. Chanéac, J. P. Jolivet, and Ph Sainctavit, J. Magn. Magn. Mater. **288**, 354 (2005).
[18]W. Q. Liu, Y. B. Xu, P. K. J. Wong, N. J. Maltby, S. P. Li, X. F. Wang, J. Du, B. You, J. Wu, P. Bencok, and R. Zhang, Appl. Phys. Lett. **104** (2014).

[19]D. J. Huang, C. F. Chang, H. T. Jeng, G. Y. Guo, H. J. Lin, W. B. Wu, H. C. Ku, A. Fujimori, Y. Takahashi, and C. T. Chen, Phys. Rev. Lett. **93**, 077204 (2004).

[20]C. T. Chen, Y. U. Idzerda, H. Lin, N. V. Smith, G. Meigs, E. Chaban, G. H. Ho, E. Pellegrin, and F. Sette, Phys. Rev. Lett. **75**, 152 (1995).

[21]V. Hari Babu, R. K. Govind, K. M. Schindler, M. Welke, and R. Denecke, J. Appl. Phys. **114** (2013).

[22]W. G. Wang, M. Li, S. Hageman, and C. L. Chien, Nat. Mater. **11**, 64 (2011).

[23]Kang L. Wang, Xufeng Kou, Pramey Upadhyaya, Yabin Fan, Qiming Shao, Guoqiang Yu, and Pedram Khalili Amiri, Proc. IEEE **104**, 1974 (2016).

[24]S. A. Wolf, D. D. Awschalom, R. A. Buhrman, J. M. Daughton, S. von Molnar, M. L. Roukes, A. Y. Chtchelkanova, and D. M. Treger, Science **294**, 1488 (2001).

[25]Yu Yan, Xianyang Lu, Bo Liu, Xiaoqian Zhang, Xiangyu Zheng, Hao Meng, Wenqing Liu, Junlin Wang, Iain G. Will, Jing Wu, Ping Kwan Johnny Wong, Jianwang Cai, Jun Du, Rong Zhang, and Yongbing Xu, J. Appl. Phys. **127** (2020).

[26]N. T. H. Kim-Ngan, A. G. Balogh, J. D. Meyer, J. Brötz, S. Hummelt, M. Zając, T. Ślęzak, and J. Korecki, Nucl. Instrum. Methods Phys. Res. B **267**, 1484 (2009).

[27]F. C. Voogt, T. T. M. Palstra, L. Niesen, O. C. Rogojanu, M. A. James, and T. Hibma, Phys. Rev. B **57**, R8107 (1998).

[28]D. T. Margulies, F. T. Parker, M. L. Rudee, F. E. Spada, J. N. Chapman, P. R. Aitchison, and A. E. Berkowitz, Phys. Rev. Lett. **79**, 5162 (1997).

[29]M. Fonin, R. Pentcheva, Yu S. Dedkov, M. Sperlich, D. V. Vyalikh, M. Scheffler, U. Rüdiger, and G. Güntherodt, Phys. Rev. B **72** (2005).

[30]M. Schmitt, O. Kirilmaz, S. Chernov, S. Babenkov, D. Vasilyev, O. Fedchenko, K. Medjanik, Yu Matveyev, A. Gloskovskii, C. Schlueter, A. Winkelmann, L. Dudy, H. J. Elmers, G. Schönhense, M. Sing, and R. Claessen, Phys. Rev. B **104** (2021).

[31]G. Mariotto, S. Murphy, and I. V. Shvets, Phys. Rev. B **66** (2002).

[32]R. Pentcheva, W. Moritz, J. Rundgren, S. Frank, D. Schrupp, and M. Scheffler, Surf. Sci. **602**, 1299 (2008).

[33]W. Wang, J. M. Mariot, M. C. Richter, O. Heckmann, W. Ndiaye, P. De Padova, A. Taleb-Ibrahimi, P. Le Fèvre, F. Bertran, F. Bondino, E. Magnano, J. Krempaský, P. Blaha, C. Cacho, F. Parmigiani, and K. Hricovini, Phys. Rev. B **87** (2013).

[34]S. Monastra, F. Manghi, C. A. Rozzi, C. Arcangeli, E. Wetli, H. J. Neff, T. Greber, and J. Osterwalder, Phys. Rev. Lett. **88**, 236402 (2002).

[35]Hui Liu, E. Y. Jiang, H. L. Bai, R. K. Zheng, and X. X. Zhang, J. Phys. D: Appl. Phys. **36**, 2950 (2003).

[36]W. Eerenstein, T. T. M. Palstra, T. Hibma, and S. Celotto, Phys. Rev. B **68** (2003).

[37]W. Eerenstein, T. T. M. Palstra, and T. Hibma, Thin Solid Films **400**, 90 (2001).

[38]K. P. McKenna, F. Hofer, D. Gilks, V. K. Lazarov, C. Chen, Z. Wang, and Y. Ikuhara, Nat. Commun. **5**, 5740 (2014).